



HAL
open science

On the Analytical Description of the Topside Ionosphere by NeQuick: Modeling the Scale Height Through COSMIC/FORMOSAT-3 Selected Data

Alessio Pignalberi, Michael Pezzopane, David Themens, Haris Haralambous,
Bruno Nava, Pierdavide Coïsson

► To cite this version:

Alessio Pignalberi, Michael Pezzopane, David Themens, Haris Haralambous, Bruno Nava, et al..
On the Analytical Description of the Topside Ionosphere by NeQuick: Modeling the Scale Height
Through COSMIC/FORMOSAT-3 Selected Data. IEEE Journal of Selected Topics in Applied Earth
Observations and Remote Sensing, 2020, 13, pp.1867-1878. 10.1109/JSTARS.2020.2986683. hal-
02896688

HAL Id: hal-02896688

<https://hal.science/hal-02896688>

Submitted on 1 Dec 2020

HAL is a multi-disciplinary open access archive for the deposit and dissemination of scientific research documents, whether they are published or not. The documents may come from teaching and research institutions in France or abroad, or from public or private research centers.

L'archive ouverte pluridisciplinaire **HAL**, est destinée au dépôt et à la diffusion de documents scientifiques de niveau recherche, publiés ou non, émanant des établissements d'enseignement et de recherche français ou étrangers, des laboratoires publics ou privés.



Distributed under a Creative Commons Attribution - NoDerivatives 4.0 International License

On the Analytical Description of the Topside Ionosphere by NeQuick: Modeling the Scale Height Through COSMIC/FORMOSAT-3 Selected Data

Alessio Pignalberi , Michael Pezzopane, David R. Themens, Haris Haralambous, Bruno Nava, and Pierdavide Coisson

Abstract—The analytical description of the topside ionosphere included in the NeQuick model is studied in detail. First, the modeled scale height behavior is analyzed at infinity and for the lowest part of the topside region; in the latter case, the analysis is done through an expansion in Taylor series near the F2-layer peak. Moreover, the significant influence of the three NeQuick topside parameters in the modeling of the topside profile is investigated in detail and, in particular, it is shown that for the lowest part of the topside the model assumes a linearly increasing trend of the topside scale height. Second, the topside formulation is inverted to derive a fully analytical expression of the topside scale height as a function of the electron density and F2-layer peak parameters. This expression has been applied to a selected and very reliable dataset of Constellation Observing System for Meteorology, Ionosphere, and Climate (COSMIC)/FORMOSAT-3 radio occultation profiles. Statistical analyses strongly support the hypothesis embedded in NeQuick regarding the linear trend of the topside scale height for the lowest part of the topside.

Index Terms—Constellation Observing System for Meteorology, Ionosphere, and Climate (COSMIC)/FORMOSAT-3 radio occultation data, NeQuick model, topside ionosphere modeling, topside scale height.

I. INTRODUCTION

THE topside part of the ionosphere extends from the height of the F2-layer peak, corresponding to the ionospheric electron density maximum ($NmF2$), to the plasmasphere [1]. Developing a reliable model of the topside ionosphere is one of the most difficult tasks because instruments commonly used

Manuscript received January 23, 2020; revised March 6, 2020; accepted March 24, 2020. Date of publication April 20, 2020; date of current version May 19, 2020. This work was supported in part by Istituto Nazionale di Geofisica e Vulcanologia, Rome, Italy and in part by the Italian MIUR-PRIN Grant 2017APKP7T on Circumterrestrial Environment: Impact of Sun–Earth Interaction. (Corresponding author: Alessio Pignalberi.)

Alessio Pignalberi and Michael Pezzopane are with the Istituto Nazionale di Geofisica e Vulcanologia, 00143 Rome, Italy (e-mail: alessio.pignalberi@ingv.it; michael.pezzopane@ingv.it).

David R. Themens is with the Department of Physics, University of New Brunswick, Fredericton, NB E3B 5A3, Canada (e-mail: david.themens@gmail.com).

Haris Haralambous is with the Frederick University, Nicosia 3080, Cyprus (e-mail: eng.hh@frederick.ac.cy).

Bruno Nava is with The Abdus Salam International Centre for Theoretical Physics, 34151, Trieste, Italy (e-mail: bnava@ictp.it).

Pierdavide Coisson is with the Université de Paris, Institut de physique du globe de Paris, CNRS, 75005, Paris, France (e-mail: coisson@ipgp.fr).

This article has supplementary downloadable material available at <https://ieeexplore.ieee.org>, provided by the authors.

Digital Object Identifier 10.1109/JSTARS.2020.2986683

to probe the ionosphere, namely ionosondes, are only capable of sounding the region below the height ($hmF2$) of the F2-layer electron density peak. Probing the topside ionosphere requires the use of more sophisticated and expensive techniques and instruments like topside sounders [2]–[4], radio occultation (RO) [5], and/or incoherent scatter radars (ISR) [6]–[9].

The topside is characterized by a, largely monotonic, decrease in the electron density as the ion population smoothly transitions from the heavy O^+ ions, dominating the lower part of the F region, to the lighter H^+ and He^+ ions above. This behavior is usually described by means of monotonically decreasing analytical functions dependent on a parameter (H_p) called topside plasma scale height [10]. An exact description of the topside plasma scale height requires knowledge of the physical state of the plasma in terms of temperature, chemical state, and mean ion mass for the whole topside profile; such accurate knowledge is, however, not currently available with the required spatial and temporal coverage. A simpler and more practical approach relies on the modeling of topside scale height by exploiting measured electron density values in order to obtain the most reliable representation of the topside vertical electron density distribution [6], [7].

The most established ionospheric models, the International Reference Ionosphere (IRI) model [11] and the NeQuick model [12] are not always able to properly represent the real features of the topside ionosphere [13]–[15]; therefore, further studies aimed at improving their topside representation are needed [16]. A part of the debate includes the choice of the mathematical function to use for the topside electron density vertical representation, the most popular being the Chapman [17] or Epstein [18], [19] families of functions [3], [20]–[22].

Since the IRI-2007 version [23], IRI has incorporated the NeQuick topside formulation [12], [14], [24] as the recommended one of its three topside options. The NeQuick topside formulation describes the topside electron density profile by means of a semi-Epstein layer with a height-dependent empirically determined topside scale height. The NeQuick topside scale height depends indeed on three parameters: H_0 , r , and g . H_0 is the scale height at the peak; r is a parameter that allows restricting the scale height increase at higher altitudes, and g is the height gradient for the scale height H_0 [25].

Recently, Pezzopane and Pignalberi [26] proposed an improvement to the topside representation of the NeQuick model

through the implementation of a new analytical formulation for the H_0 parameter used by the model to calculate the topside scale height. To accomplish this task, they fitted the NeQuick topside analytical function through two anchor points: the F2-layer absolute electron density maximum and the electron density value as measured by Swarm satellites [27], [28].

Themens *et al.* [29] demonstrated that the NeQuick topside model does not succeed in capturing the curvature of the topside at high and upper-mid latitudes. In that study and furthermore in [30], they showed that the parameters used by the NeQuick and IRI to model H_0 are not able to fully describe the seasonal and diurnal variability of H_0 in these regions. Furthermore, they confirmed that a revision of the choice of r and g parameters was necessary for the application to mid- and high-latitude regions. For their purposes, an r value of 20 and g value of 0.2024 was found to optimally represent the curvature of the topside profile. Also, in [29], the behavior of the topside scale height and the roles of the r and g parameters were presented, but without explaining in details the procedure applied to obtain the relevant results. In this study, we will thoroughly explain the process by which the relationships presented in [29] were derived and further explain the implications of these relationships with respect to electron density.

Specifically, the NeQuick topside scale height formulation is mathematically studied to highlight some of its features. In particular, we here expand the semi-Epstein layer formulation around $hmF2$ through the Taylor series to explain the effect of H_0 , r , and g parameters in the lower topside. The asymptotic behavior at infinity is also presented. In this way, we aim to complement the published literature about the NeQuick topside formulation.

In addition, we show how it is possible to analytically invert the semi-Epstein formulation (on which the NeQuick topside is based) to derive the topside scale height as a function of measured parameters. This new methodology has been applied to a dataset of selected Constellation Observing System for Meteorology, Ionosphere, and Climate (COSMIC) RO profiles to calculate the topside scale height and then to model it by considering a linear dependence on the altitude. The linear dependence, validated against COSMIC topside profiles, is shown to be appropriate to model the lower part of the topside but fails to capture the behavior of the topside at high altitudes.

II. MATHEMATICAL DESCRIPTION OF THE NEQUICK TOPSIDE MODEL

A. NeQuick Topside

Since the NeQuick model was designed to allow fast calculation of TEC up to global navigation satellite systems (GNSS) heights, the topside was designed to allow a transition from the altitude variation near the electron density peak to the plasmaspheric one, without the inclusion of an additional transition height model [20].

The NeQuick topside analytical formulation has evolved from its original formulation [20] to the current NeQuick 2 version [12], [14]. It now consists of a semi-Epstein layer describing the topside electron density N_e as a function of the height h , starting

from the $NmF2$ value at the $hmF2$ height

$$N_e(h) = 4NmF2 \frac{\exp\left(\frac{h-hmF2}{H}\right)}{\left[1 + \exp\left(\frac{h-hmF2}{H}\right)\right]^2} \quad (1)$$

the electron density decrease with height is driven by a modeled scale height H

$$H(h) = H_0 \left[1 + \frac{rg(h-hmF2)}{rH_0 + g(h-hmF2)} \right]. \quad (2)$$

NeQuick describes the scale height as a function of three empirically deduced parameters: H_0 , g , and r . H_0 is the value assumed by the scale height at the F2-layer peak height ($H = H_0$ when $h = hmF2$), whereas $g = 0.125$ and $r = 100$ [12], [20].

r and g parameters have been empirically set to constant values, whereas H_0 is modeled as a function of the bottomside thickness parameter, solar activity index, and other bottomside parameters [12], [14]. In this way, the topside scale height (2) is strongly coupled to the bottomside profile through the H_0 formulation. However, in many cases, the topside ionosphere exhibits different behavior when compared with the bottomside one [29], [30], which means that modeling the topside region through only bottomside parameters could lead to inaccurate results.

B. NeQuick Topside Scale Height Behavior Near the F2-Layer Peak

The behavior of the NeQuick topside scale height just above the F2-layer peak can be studied by expanding it in a Taylor series around $hmF2$.

Making the variable change $z = h - hmF2$, (2) can be written as

$$H(z) = H_0 + rgH_0 \left(\frac{z}{rH_0 + gz} \right). \quad (3)$$

In (3), the only term dependent on the reduced height z is

$$f(z) = \frac{z}{rH_0 + gz} \quad (4)$$

$f(z)$ is the term to be expanded in Taylor series around $z = z_0 = 0$ (i.e., for $h = hmF2$).

In this way, the topside scale height is described by

$$H(z) \simeq H_0 + rgH_0 \sum_{n=1}^{\infty} \frac{1}{n!} \frac{\partial^n f(z_0)}{\partial z^n} (z - z_0)^n \quad (5)$$

where H_0 represents the zeroth-order term.

The first four derivatives of $f(z)$ are

$$\begin{cases} \frac{\partial f(z)}{\partial z} = \frac{rH_0}{(rH_0 + gz)^2} \\ \frac{\partial^2 f(z)}{\partial z^2} = -\frac{2rgH_0}{(rH_0 + gz)^3} \\ \frac{\partial^3 f(z)}{\partial z^3} = \frac{6rg^2H_0}{(rH_0 + gz)^4} \\ \frac{\partial^4 f(z)}{\partial z^4} = -\frac{24rg^3H_0}{(rH_0 + gz)^5} \end{cases}. \quad (6)$$

From (6), by mathematical induction, we deduce that

$$\frac{\partial^n f(z)}{\partial z^n} = (-1)^{n-1} \frac{n!rg^{n-1}H_0}{(rH_0 + gz)^{n+1}}. \quad (7)$$

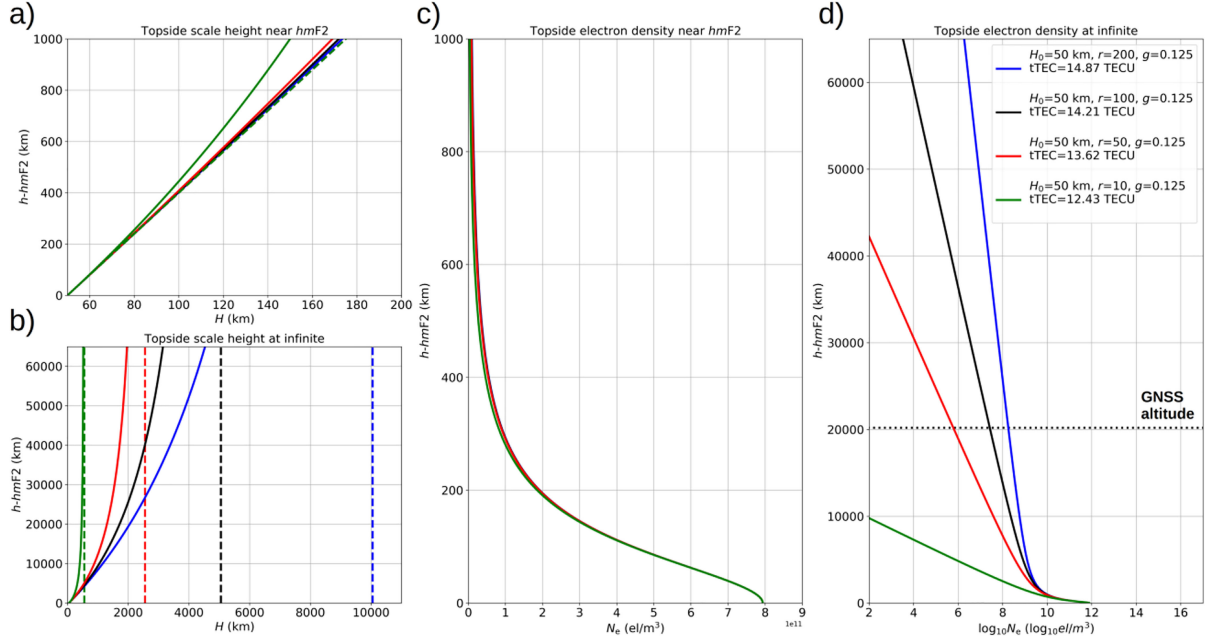


Fig. 1. (a) Topside scale height dependence on the altitude near $hmF2$. (b) Corresponding asymptotic behavior at infinity. (c) Topside electron density profile near $hmF2$. (d) Corresponding asymptotic behavior at infinity. Colors represent values obtained for different r values ($r = 200$, blue; $r = 100$, black; $r = 50$, red; $r = 10$, green) with g and H_0 kept constant to 0.125 and 50 km, respectively. In panels (c) and (d), $foF2 = 8$ MHz, that is $NmF2 \approx 7.94 \cdot 10^{11} \text{el/m}^3$, a typical daytime value at midlatitudes for midsolar activity levels. The dashed lines in panel (a) represent the asymptotic behavior near $hmF2$ [see (11)], whereas dashed lines in panel (b) represent the asymptotic behavior at infinity [see (14)]. In panel (d), tTEC values are calculated from $hmF2$ to the GNSS satellites altitude (20 200 km, represented by a dotted horizontal line).

Substituting (7) into (5), we obtain

$$H(z) \simeq H_0 + rgH_0 \sum_{n=1}^{\infty} (-1)^{n-1} \frac{rg^{n-1}H_0}{(rH_0 + gz_0)^{n+1}} (z - z_0)^n \quad (8)$$

and setting $z_0 = 0$

$$\begin{aligned} H(z) &\simeq H_0 + rgH_0 \sum_{n=1}^{\infty} (-1)^{n-1} \frac{rg^{n-1}H_0}{(rH_0)^{n+1}} (z)^n \\ &= H_0 + \sum_{n=1}^{\infty} (-1)^{n-1} \frac{g^n}{(rH_0)^{n-1}} (z)^n. \end{aligned} \quad (9)$$

Redefining in (9) the index of the series as $i = n - 1$, and coming back to the real height h , (9) becomes

$$H(h) \simeq H_0 + \sum_{i=0}^{\infty} (-1)^i \frac{g^{i+1}}{(rH_0)^i} (h - hmF2)^{i+1}. \quad (10)$$

Equation (10) describes how the topside scale height depends on height just above $hmF2$.

By considering only the first-order approximation of (10) (i.e., for $i = 0$), we obtain

$$H(h) \simeq H_0 + g(h - hmF2). \quad (11)$$

Equation (11) shows that at the first-order of approximation, the topside scale height exhibits a linear dependence on the reduced height, with H_0 representing the intercept and g the slope. This is coherent with the interpretation of Themens *et al.* [29].

C. NeQuick Topside Scale Height Behavior as the Height Approaches Infinity

The behavior of the NeQuick topside scale height as the height approaches infinity can be easily studied through (3)

$$\lim_{z \rightarrow \infty} H(z) = H_0 + rgH_0 \lim_{z \rightarrow \infty} \frac{z}{rH_0 + gz}. \quad (12)$$

Equation (12) can be resolved by applying the de L'Hôpital's rule as follows:

$$\lim_{z \rightarrow \infty} \frac{z}{rH_0 + gz} = \lim_{z \rightarrow \infty} \frac{\frac{\partial}{\partial z}(z)}{\frac{\partial}{\partial z}(rH_0 + gz)} = \lim_{z \rightarrow \infty} \frac{1}{g} = \frac{1}{g}. \quad (13)$$

Substituting (13) into (12), we obtain

$$H(z) \simeq H_0(1 + r). \quad (14)$$

Equation (14) shows that the parameter r of the NeQuick topside scale height formulation controls the asymptotic behavior of the scale height. Themens *et al.* [29] followed the same approach to express the asymptotic behavior of H at high altitudes.

D. Impact of r , g , and H_0 on the Topside Profile Shape

In this section, we aim at visually showing how different values of the parameters r , g , and H_0 affect the topside profile shape, both near the F2-layer peak and at altitudes approaching infinity. For this purpose, we used (2).

In Fig. 1, we have kept constant g and H_0 and varied r . Fig. 1(a) and (b) shows the dependence of H on the reduced height $z = h - hmF2$ (solid lines), for the first 1000 km above $hmF2$ and very distant from $hmF2$ (virtually at infinity). Fig. 1(c) and (d)

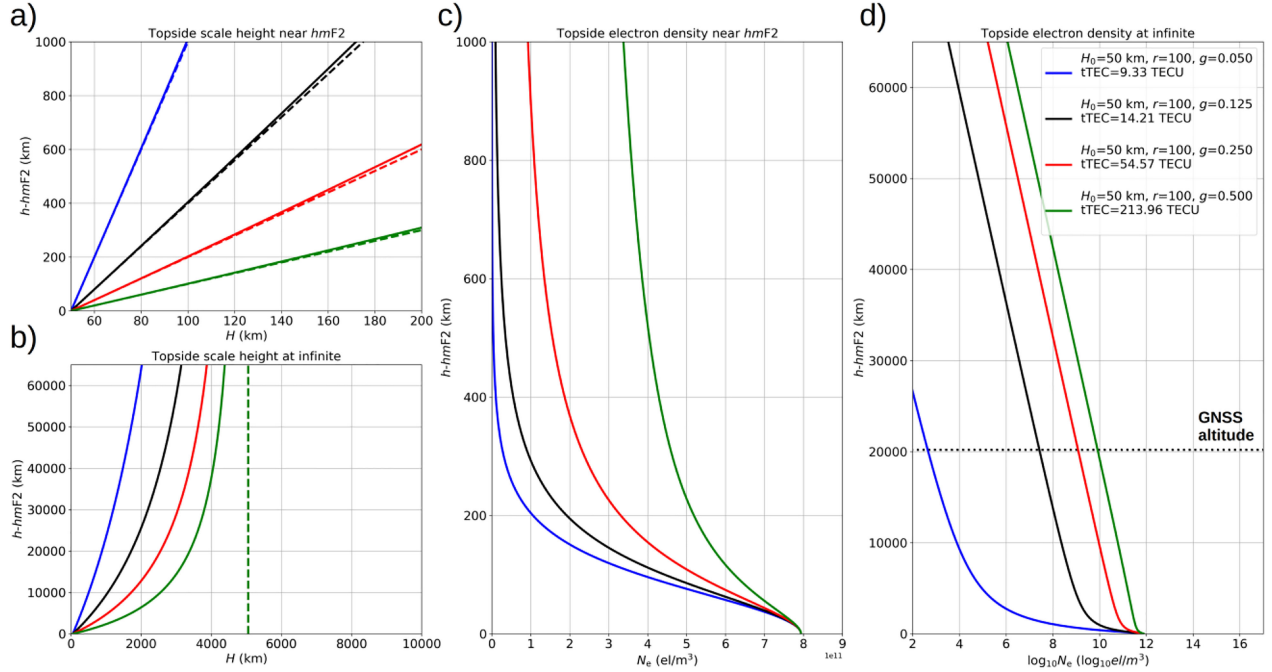


Fig. 2. Same as Fig. 1 but for different g values ($g = 0.050$, blue; $g = 0.125$, black; $g = 0.250$, red; $g = 0.500$, green) and keeping constant r and H_0 to 100 and 50 km, respectively.

shows the dependence of the electron density on the reduced height calculated by putting (2) in (1), near $hmF2$ and at infinity. Fig. 1(a) and (c) shows that the r parameter has a marginal effect on the topside profile near $hmF2$, whereas it has a major impact on the topside profile at infinity, as depicted in Fig. 1(b) and (d). In particular, the parameter r describes how rapidly N_e goes to zero at infinity [see Fig. 1(d)]. The higher the value of r , the higher H is at a fixed altitude [see Fig. 1(a) and (b)], and correspondingly, the higher N_e is at a fixed altitude [see Fig. 1(c) and (d)], and the higher the topside total electron content (tTEC) is.

The behavior of the topside NeQuick very far from the F2-layer peak can be analyzed by studying (1) near infinity

$$\lim_{z \rightarrow \infty} N_e(z) = \lim_{z \rightarrow \infty} 4NmF2 \frac{\exp\left(\frac{z}{H}\right)}{\left[1 + \exp\left(\frac{z}{H}\right)\right]^2}. \quad (15)$$

Equation (15) can be solved by applying the de L'Hôpital's rule as follows:

$$\begin{aligned} \lim_{z \rightarrow \infty} 4NmF2 \frac{\exp\left(\frac{z}{H}\right)}{\left[1 + \exp\left(\frac{z}{H}\right)\right]^2} &= 4NmF2 \lim_{z \rightarrow \infty} \frac{\frac{\partial}{\partial z} \left[\exp\left(\frac{z}{H}\right)\right]}{\frac{\partial}{\partial z} \left\{\left[1 + \exp\left(\frac{z}{H}\right)\right]^2\right\}} \\ &= 2NmF2 \lim_{z \rightarrow \infty} \frac{1}{1 + \exp\left(\frac{z}{H}\right)}. \end{aligned} \quad (16)$$

Obviously, (16) confirms that N_e goes to zero at infinity but, more importantly, N_e decays like an exponential, representing a

radial diffusive equilibrium for a single ion species [31]

$$\begin{aligned} N_e(z \rightarrow \infty) &\simeq 2NmF2 \exp\left(-\frac{z}{H(z \rightarrow \infty)}\right) \\ &\simeq 2NmF2 \exp\left(-\frac{z}{H_0(1+r)}\right). \end{aligned} \quad (17)$$

Equation (17) indicates that increasing the parameter r (with H_0 fixed), the electron density at infinity increases significantly [see Fig. 1(d)].

By taking the logarithm in base 10 of (17), we get

$$\log_{10} N_e(z \rightarrow \infty) \simeq \log_{10} 2NmF2 - \frac{1}{\ln 10} \frac{z}{H_0(1+r)}. \quad (18)$$

From (18), it is clear that the slope of $\log_{10} N_e(z \rightarrow \infty)$ shown in Fig. 1(d) (apart from the constant factor $1/\ln 10$) depends on $H_0(1+r)$ and, thus, on both the H_0 and r parameters.

In Fig. 2 we have kept constant r and H_0 and varied g . From Fig. 2(a) and (c), we can see how the g parameter significantly affects the topside profile near $hmF2$. In particular, the parameter g describes the slope of H near $hmF2$, as described by (11). The higher is the g value, the higher is H at a fixed altitude [see Fig. 2(a) and (b)], and then the higher is N_e at a fixed altitude [see Fig. 2(c) and (d)]. From Fig. 2(d), we can see that g does not affect the slope of N_e at high altitudes when represented in a logarithmic scale, as described by (18).

In Fig. 3, we have kept constant g and r and varied H_0 . From Fig. 3(a) and (c), we can see how the H_0 parameter has a significant impact on the topside profile both near $hmF2$ [as depicted in Fig. 3(a) and (c)] and at infinity [as depicted in Fig. 3(b) and (d)]. In particular, the parameter H_0 represents the

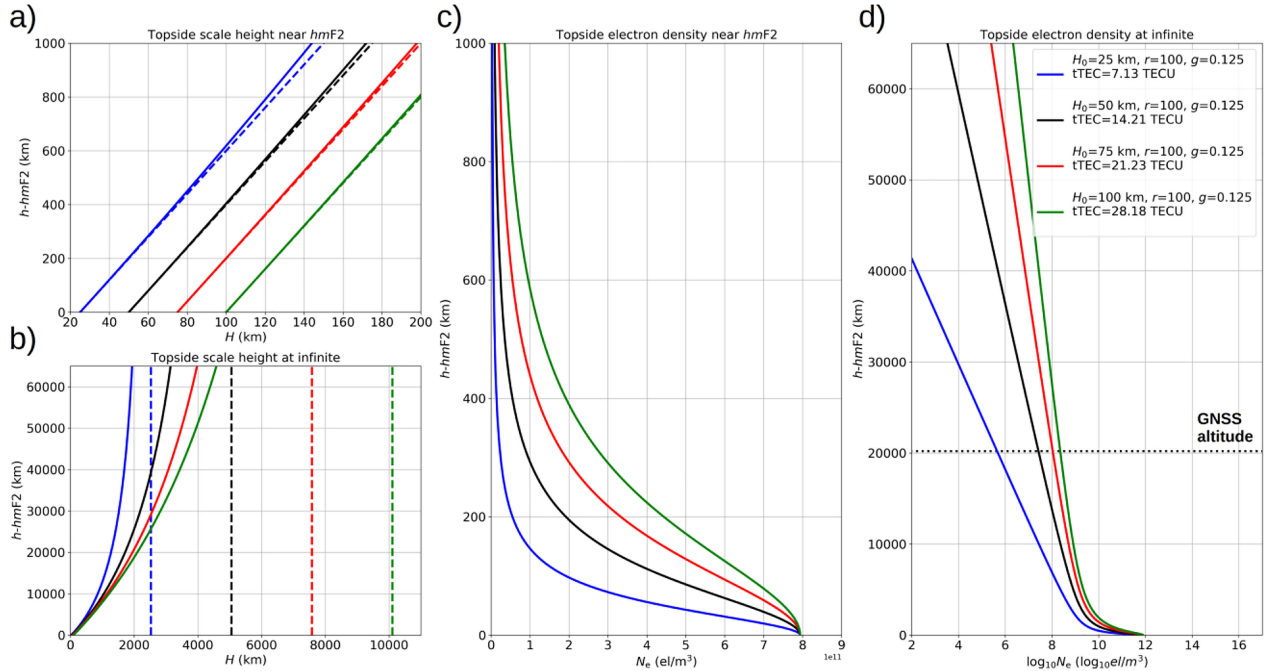


Fig. 3. Same as Fig. 1 but for different H_0 values ($H_0 = 25$ km, blue; $H_0 = 50$ km, black; $H_0 = 75$ km, red; $H_0 = 100$ km, green) and keeping constant g and r to 0.125 and 100, respectively.

intercept of H at $hmF2$, and considering (11) and (14), it affects the overall topside profile shape. The higher the H_0 value, the higher H is at a fixed altitude [see Fig. 3(a) and (b)], and then the higher N_e is at a fixed altitude [see Fig. 3(c) and (d)].

Since the parameter H_0 affects both the topside behavior near $hmF2$ (like the g parameter) and at infinity (like the r parameter) one should pay particular attention to its modeling. This is why the update of NeQuick model [12], [14] and its recent correction (NeQuick-corr [26]) focus on both the modeling of H_0 .

III. TOPSIDE MODELING THROUGH COSMIC/FORMOSAT-3 RO DATA

A. COSMIC/FORMOSAT-3 RO Dataset Selection

COSMIC/FORMOSAT-3 is a constellation made up of six microsattellites launched on April 15, 2006 into a circular orbit (with 72° of inclination) at about 800 km altitude and a separation angle of 30° in longitude between neighboring satellites [32]. The mission is a collaborative project between the National Space Organization in Taiwan and the University Corporation for Atmospheric Research in the United States. Each satellite carries a global positioning system (GPS) RO receiver capable of measuring the phase delay of radio waves from GPS satellites as they are occulted by the Earth's atmosphere and thus providing an accurate determination of the ionospheric vertical electron density profile [33], [34].

The calculation of the topside scale height requires very reliable topside profiles. In order to perform our investigation using topside RO profiles under the best possible collocation conditions with corresponding ionosondes, in space and time,

we have compiled a very reliable dataset by selecting RO COSMIC profiles collocated (within 1° in latitude and longitude) and simultaneous (within 7.5 min) with ionosonde measured profiles for which both $NmF2_{COSMIC} \approx NmF2_{IONOSONDE}$ and $hmF2_{COSMIC} \approx hmF2_{IONOSONDE}$ matched within 5%. Ionosonde data used in this study were downloaded from the Digital Ionogram DataBASE by means of the SAO Explorer software developed by the University of Massachusetts, Lowell [35]. To maximize the accuracy, only manually scaled ionograms were used to obtain the electron density profiles.

In standard RO data inversion, the inversion error is systematically accumulated from the top of the RO inverted profile to the bottom; thus, when $NmF2_{COSMIC}$ matches $NmF2_{IONOSONDE}$, it is expected that the full topside of the RO profile is correctly estimated [36].

According to these constraints, we were able to select 382 profiles over selected ionosonde stations (see Table I), from 2006 to 2015. The spatial distribution and the number of selected COSMIC profiles are provided in the bubbleplot of Fig. 4.

B. Calculation of the Topside Scale Height Through COSMIC/FORMOSAT-3 RO Profiles

For each of the 382 selected RO profiles, only the topside part is considered, namely from $hmF2$ to the altitude of the COSMIC satellite (between 700 and 800 km, depending on the geometry of the RO path). Because RO-derived topside electron density values are unevenly distributed with height, they were linearly interpolated to obtain profiles with a 1-km step in height.

TABLE I
IONOSONDE STATIONS COLLOCATED WITH COSMIC RO PROFILES

| Station name (country) | Geog. Lat. (°) | Geog. Lon. (°) | QD Mag. Lat. (°) | # of profiles |
|------------------------------|----------------|----------------|------------------|---------------|
| Ascension Island (UK) | -7.95 | 345.60 | -18.28 | 3 |
| Athens (Greece) | 38.00 | 23.50 | 31.98 | 21 |
| Boulder (USA) | 40.00 | 254.70 | 48.35 | 7 |
| Cachoeira Paulista (Brazil) | -22.70 | 315.00 | -18.47 | 4 |
| Chilton (UK) | 51.50 | 359.40 | 47.83 | 31 |
| College AK (USA) | 64.90 | 212.00 | 65.00 | 6 |
| Dourbes (Belgium) | 50.10 | 4.60 | 45.90 | 30 |
| Dyess AFB (USA) | 32.40 | 260.20 | 41.56 | 1 |
| Eglin AFB (USA) | 30.50 | 273.50 | 41.08 | 13 |
| El Arenosillo (Spain) | 37.10 | 353.30 | 30.82 | 9 |
| Fairford (UK) | 51.70 | 358.50 | 48.13 | 9 |
| Fortaleza (Brazil) | -3.90 | 321.60 | -6.41 | 3 |
| Gakona (USA) | 62.38 | 215.00 | 62.99 | 3 |
| Goose Bay (Canada) | 53.50 | 299.70 | 60.46 | 2 |
| Grahamstown (South Africa) | -33.30 | 26.50 | -41.38 | 18 |
| Jeju (South Korea) | 33.43 | 126.30 | 26.81 | 2 |
| Jicamarca (Peru) | -12.00 | 283.20 | 0.09 | 2 |
| Juliusruh (Germany) | 54.60 | 13.40 | 50.71 | 21 |
| King Salmon (USA) | 58.40 | 203.60 | 56.89 | 2 |
| Kwajalein (Marshall isl.) | 9.00 | 167.20 | 3.85 | 2 |
| Learmonth (Australia) | -21.80 | 114.10 | -32.25 | 8 |
| Louisvale (South Africa) | -28.50 | 21.20 | -37.67 | 8 |
| Madimbo (South Africa) | -22.39 | 30.88 | -32.33 | 16 |
| Millstone Hill (USA) | 42.60 | 288.50 | 51.77 | 16 |
| Moscow (Russia) | 55.47 | 37.30 | 51.34 | 18 |
| Narsarsuaq (Greenland) | 61.20 | 314.60 | 65.42 | 1 |
| Nicosia (Cyprus) | 35.03 | 33.16 | 29.23 | 9 |
| Port Stanley (Falkland isl.) | -51.60 | 302.10 | -38.88 | 10 |
| Pruhonice (Czech Republic) | 50.00 | 14.60 | 45.49 | 26 |
| Point Arguello (USA) | 34.80 | 239.50 | 40.31 | 9 |
| Qaanaaq (Greenland) | 77.50 | 290.80 | 84.54 | 1 |
| Ramey (Puerto Rico) | 18.50 | 292.80 | 27.59 | 8 |
| Rome (Italy) | 41.80 | 12.50 | 36.03 | 12 |
| Roquetes (Spain) | 40.80 | 0.50 | 34.98 | 11 |
| San Vito (Italy) | 40.60 | 17.80 | 34.73 | 15 |
| Sao Luis (Brazil) | -2.60 | 315.80 | -2.27 | 6 |
| Sondrestrom (Greenland) | 66.98 | 309.06 | 72.28 | 1 |
| Tromso (Norway) | 69.60 | 19.20 | 66.52 | 7 |
| Wallops Island (USA) | 37.94 | 284.42 | 47.83 | 3 |
| Yakutsk (Russia) | 62.00 | 129.60 | 56.33 | 8 |
| Total | | | | 382 |

Note. The geographical location (geographic latitude and longitude) and the magnetic location (quasi-dipole magnetic latitude at 350 km of altitude [37]), along with the number of selected profiles, are shown.

To calculate topside scale height values, the Epstein function (1) is analytically inverted as follows:

$$N_e(h) = 4NmF2 \frac{\exp\left(\frac{h-hmF2}{H}\right)}{\left[1 + \exp\left(\frac{h-hmF2}{H}\right)\right]^2}$$

$$\Rightarrow \frac{N_e(h)}{4NmF2} = \frac{\exp\left(\frac{h-hmF2}{H}\right)}{\left[1 + \exp\left(\frac{h-hmF2}{H}\right)\right]^2}. \quad (19)$$

by making the following variables change

$$\begin{cases} t = \exp\left(\frac{h-hmF2}{H}\right) \\ \alpha = \frac{N_e(h)}{4NmF2} \end{cases}. \quad (20)$$

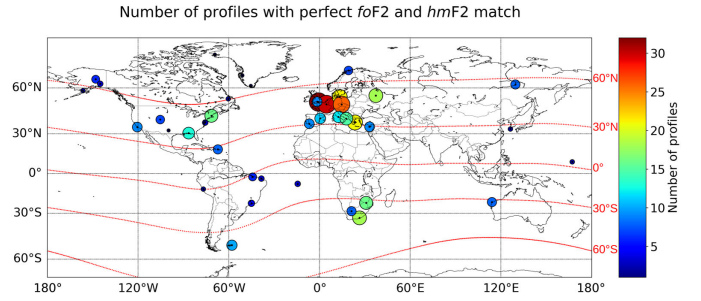


Fig. 4. Bubbleplot representing the spatial distribution and the number of selected COSMIC RO profiles according to Table I. Red dotted lines represent quasi-dipole magnetic latitude isolines.

Equation (19) becomes

$$\alpha = \frac{t}{1 + 2t + t^2} \Rightarrow \alpha t^2 + (2\alpha - 1)t + \alpha = 0. \quad (21)$$

Equation (21) is a quadratic equation in the variable t that can be easily solved to obtain the following two solutions:

$$\begin{cases} t_1(h) = \frac{1}{N_e(h)} \left[(2NmF2 - N_e(h)) + 2\sqrt{NmF2^2 - N_e(h) \cdot NmF2} \right] \\ t_2(h) = \frac{1}{N_e(h)} \left[(2NmF2 - N_e(h)) - 2\sqrt{NmF2^2 - N_e(h) \cdot NmF2} \right] \end{cases}. \quad (22)$$

Inverting t from (20) to obtain the scale height H , we get

$$H_{1,2}(h) = \frac{h - hmF2}{\ln[t_{1,2}(h)]}. \quad (23)$$

Analytically, two solutions for H are possible: the one corresponding to t_1 , and the other one corresponding to t_2 . It can be easily verified from (22) that $t_1 \geq 1$ and $0 \leq t_2 \leq 1$ in the topside (where $N_e(h) \leq NmF2$); by putting t_1 and t_2 in (23), we can verify that in the topside (where $h \geq hmF2$) $H_1 \geq 0$ and $H_2 \leq 0$, despite being equal in magnitude $\|H_1\| = \|H_2\|$. Even though both are solutions mathematically acceptable, because the semi-Epstein function (1) is even (thus symmetric) with respect to $h-hmF2$, we reject t_2 because it produces negative values of H .

Thus, the topside scale height that will be used in this work is the one corresponding to t_1 , which for simplicity we name H_{Epstein} from now on, as follows:

$$H_{\text{Epstein}}(h) = \frac{h - hmF2}{\ln\left\{\frac{1}{N_e(h)} \left[(2NmF2 - N_e(h)) + 2\sqrt{NmF2^2 - N_e(h) \cdot NmF2} \right]\right\}}. \quad (24)$$

By applying (24), it is possible to calculate the topside scale height for each height h by using measured $N_e(h)$, $NmF2$, and $hmF2$ values. An example of this procedure applied to COSMIC-derived parameters is shown in Fig. 5. Blue points in the bottom panel of Fig. 5 are topside scale height values H_{Epstein} calculated by applying (24) to COSMIC measured electron density values, shown as blue points in the top panel of Fig. 5.

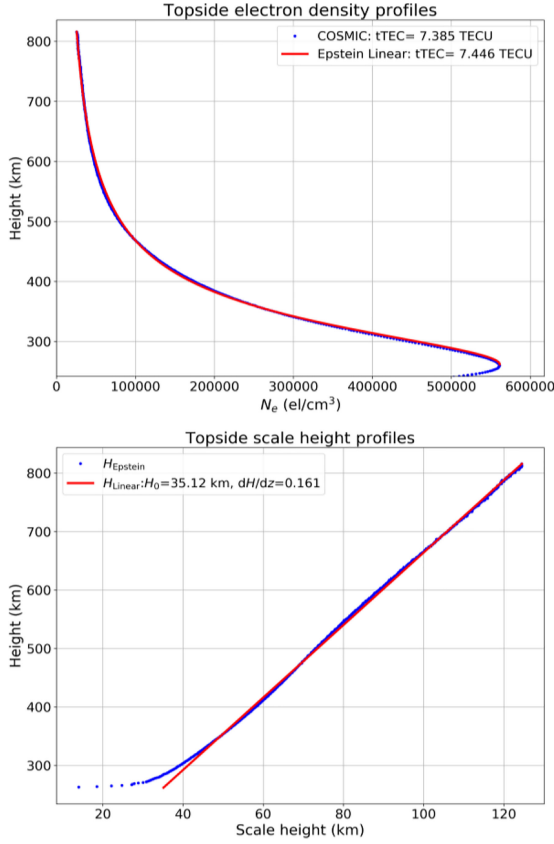


Fig. 5. (Top panel) Topside electron density values (blue points) measured by COSMIC and (red line) modeled by using the topside scale height H_{Linear} , as defined in the bottom panel. (Bottom panel) Topside scale height values (H_{Epstein} , blue points) obtained from the COSMIC measured profile shown in the top panel, and corresponding modeling through a linear fit (H_{Linear} , red line). The COSMIC profile is the one measured on September 11, 2010 at 16:16:24 universal time (UT) at Lat = 33.44°N and Lon = 30.24°E.

Looking at calculated H_{Epstein} values, a clear linear dependence with height can be seen. We verified that such linear behavior is a feature shared by most of the selected COSMIC RO profiles used in this study; further studies are underway to verify whether this is a definite feature of the topside ionosphere, at least for the altitudinal range probed by COSMIC satellites. This is why a linear fit of calculated $H_{\text{Epstein}}(h)$ values has been performed for the altitudinal range $[hmF2+50; h_{\text{COSMIC}}-20]$ km. The first 50 km above $hmF2$ were discarded because in some cases the Epstein formulation (1) is not able to properly reproduce the F2-layer curvature near the peak. The last 20 km below the COSMIC height (h_{COSMIC}) were instead not considered to avoid errors that could arise due to the geometric configuration of ray-paths nearly parallel to the satellite movement.

The fitted topside scale height obtained with this procedure is

$$H_{\text{Linear}}(z) = \frac{\partial H_{\text{Linear}}}{\partial z} z + H_{0,\text{Linear}} \quad (25)$$

where $z = h - hmF2$ and

$$H_{0,\text{Linear}} = H_{\text{Linear}}(z = 0) = H_{\text{Linear}}(h = hmF2). \quad (26)$$

Equation (25) describes the modeled topside scale height H_{Linear} dependence on the reduced height z obtained through the linear fit procedure applied on calculated $H_{\text{Epstein}}(h)$ values.

The linear fit procedure outputs the slope and the intercept of $H_{\text{Linear}}(z)$. The slope $\frac{\partial H_{\text{Linear}}}{\partial z}$ represents the gradient of the modeled topside scale height, whereas the intercept $H_{0,\text{Linear}}$ represents the value of H_{Linear} when $h = hmF2$.

By comparing (11) and (25), we obtain

$$\begin{cases} g \equiv \frac{\partial H}{\partial z} \\ H_0 \equiv H_{0,\text{Linear}} \end{cases} \quad (27)$$

An example of the linear fit performed on $H_{\text{Epstein}}(h)$ values is shown at the bottom panel of Fig. 5. Modeled topside electron density values are calculated by inserting in (1) H_{Linear} values in place of H and are represented by the red curve in the top panel of Fig. 5. The comparison between electron density values measured by COSMIC and those modeled by using H_{Linear} testifies that it is possible to accurately reproduce the ionospheric topside electron density profile by using a semi-Epstein layer with a scale height linearly dependent on height, at least from $hmF2$ to about 800 km of height. This largely agrees with previous works using a Chapman function with height-varying scale height [2], [38]–[40].

The interested reader can find plots for each selected RO profile (like the one in Fig. 5), used in the following statistical analysis, in the Supplementary Material.

IV. RESULTS AND DISCUSSION

A. Statistical Validation of the Topside Scale Height Linear Approximation

For each of the selected COSMIC RO profiles, tTEC is calculated by integrating topside electron density values from $hmF2$ to the satellite height as follows:

$$t\text{TEC}_{\text{measured}} = \int_{hmF2}^{h_{\text{COSMIC}}} N_{e,\text{COSMIC}} dh. \quad (28)$$

Moreover, each topside RO profile provides measured values of $NmF2$ and $hmF2$ that are used to model the topside profile through (1) with H_{Linear} values obtained applying (25) to H_{Epstein} values calculated through (24) for the considered RO profile, as described in Section III-B.

tTEC modeled values are then calculated as follows:

$$t\text{TEC}_{\text{modeled}} = \int_{hmF2}^{h_{\text{COSMIC}}} N_{e,\text{Epstein Linear}} dh. \quad (29)$$

Then, tTEC root mean square error (RMSE) and normalized RMSE (NRMSE) values were calculated, expressed in TECU (1 TECU = 10^{16} el/m²) and in percentage, for the entire selected COSMIC dataset

$$\begin{aligned} \text{RMSE}[\text{TECU}] &= \sqrt{\frac{\sum_{i=1}^N (t\text{TEC}_{\text{modeled},i} - t\text{TEC}_{\text{measured},i})^2}{N}} \quad (30) \end{aligned}$$

$$\begin{aligned} \text{NRMSE}[\%] &= \sqrt{\frac{\sum_{i=1}^N \left(\frac{t\text{TEC}_{\text{modeled},i} - t\text{TEC}_{\text{measured},i}}{t\text{TEC}_{\text{measured},i}} \cdot 100 \right)^2}{N}} \quad (31) \end{aligned}$$

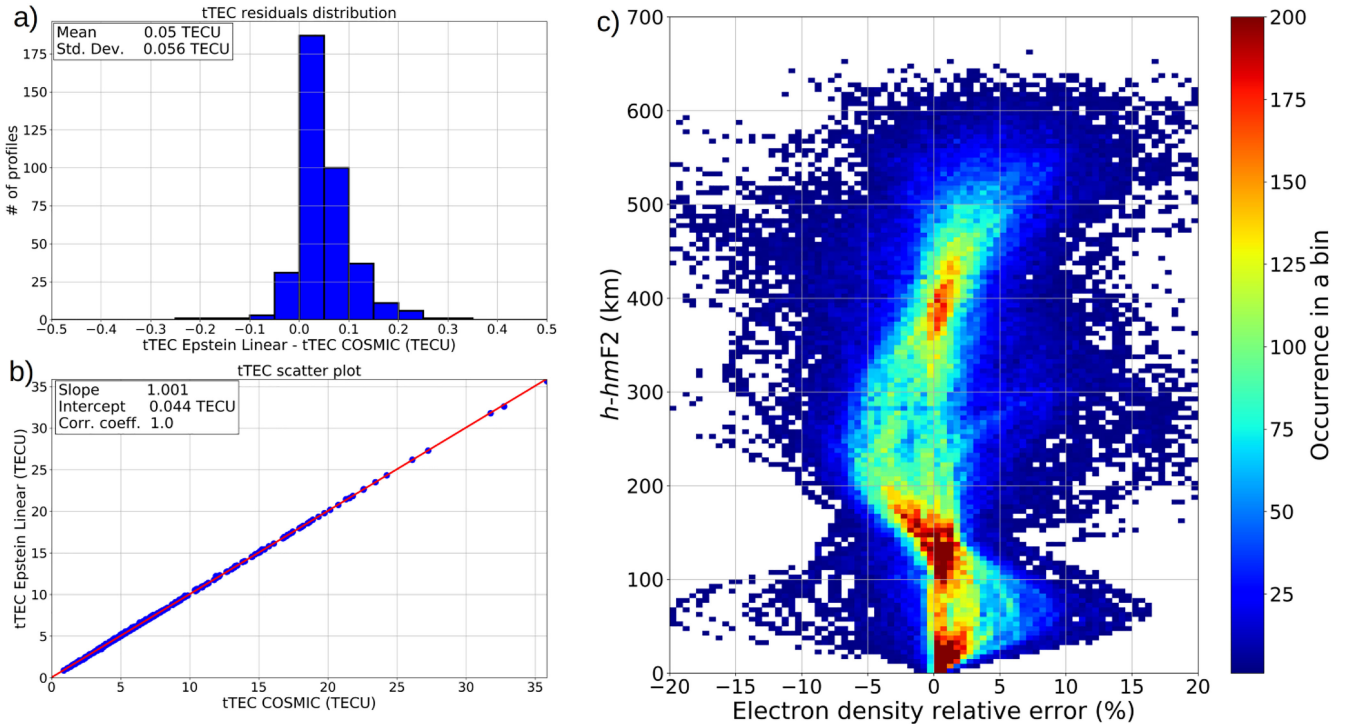


Fig. 6. (a) Histogram of residuals between tTEC values modeled by the Epstein Linear formulation and COSMIC measured ones. (b) Scatter plot of tTEC values modeled by the Epstein Linear formulation and COSMIC measured ones. Red line represents the best linear fit line. (c) Density plot of residuals percentage between modeled (by Epstein Linear) and measured (by COSMIC) electron density values as a function of the reduced height.

where $N = 382$ and runs on the selected COSMIC profiles.

We obtained the following statistical values: RMSE = 0.070 TECU and NRMSE = 1.389% using all 382 COSMIC profiles.

Fig. 6(a) and (b) shows, respectively, the histogram of residuals between topside tTEC values modeled through the Epstein Linear formulation and COSMIC measured ones and a scatter plot of the modeled and measured tTEC values. Fig. 6(a) shows that the distribution of residuals is well peaked around zero (residuals mean = 0.050 TECU) with a very low dispersion (residuals standard deviation = 0.056 TECU). Similar considerations can be drawn from the scatter plot that exhibits a one-to-one dependence between measured and modeled tTEC values (slope = 1.001, intercept = 0.044 TECU, Pearson correlation coefficient = 1.0).

Statistics on tTEC values gives an overall picture of performance for the whole topside profile; however, it is also interesting to show how residuals of the electron density are distributed as a function of height. Fig. 6(c) presents a density plot of percentage residuals between modeled ($N_{e,Epstein\ Linear}$) and measured ($N_{e,COSMIC}$) electron density values as a function of the reduced height z , which is calculated as follows:

$$\begin{aligned} \text{Electron density relative error } (z)[\%] \\ = \frac{N_{e,Epstein\ Linear}(z) - N_{e,COSMIC}(z)}{N_{e,COSMIC}(z)} \cdot 100 \end{aligned} \quad (32)$$

this figure shows that most of the percentage error lies within 5% for the whole topside profile probed by COSMIC satellites.

B. Some Caveats of the Applied Methodology

The case shown in Fig. 5 represents a very good example, exhibiting a good linear dependence of the topside scale height on height for the entire COSMIC topside profile; however, there are some cases, characterized by slight departures from the linear behavior, that need to be highlighted.

Fig. 7(a) refers to a COSMIC RO profile measured near the equator (geographical latitude = 2.38°S, quasi-dipole magnetic latitude = 0.90°S) at 14:00 local time (LT). From Fig. 7(b), it is clear how the topside scale height calculated through the linear approximation (25) cannot properly reproduce the scale height behavior just above $hmF2$, causing an error in the estimation of H_0 . A similar behavior is also exhibited by the profile of Fig. 7(c), measured at high latitudes (geographical latitude = 65.19°N, quasi-dipole magnetic latitude = 64.84°N) at 10:00 LT. In this case, Fig. 7(d) shows very good linear behavior between 300 and 700 km of height and an evident departure from it above (probably due to artifacts), which produces an error in the estimation of the scale height gradient and intercept. Most of the cases for which the calculated topside scale height exhibits a slight departure from the linear trend concern COSMIC profiles retrieved at low latitudes. This is probably due to the assumption of spherical symmetry made by the Abel inversion procedure used to obtain COSMIC electron density profiles. Indeed, this hypothesis is hardly satisfied in the equatorial ionization anomaly region, where strong horizontal electron density gradients arise, and then causing errors in the retrieving procedure [41]–[43].

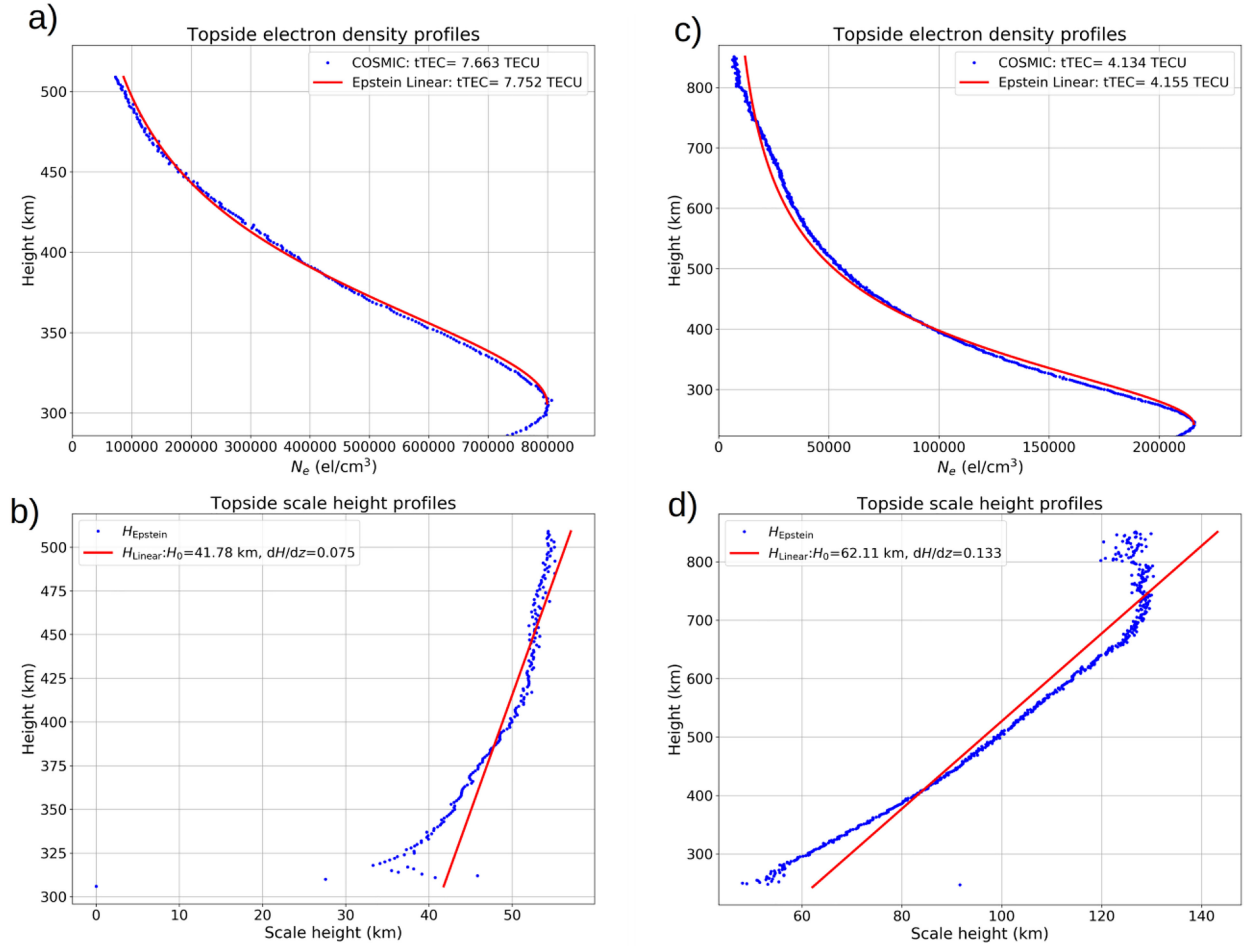


Fig. 7. Same as Fig. 5 but (a) and (b) for the COSMIC profile measured on June 24, 2006 at 17:14:12 UT at Lat = 2.38°S and Lon = 45.43°W and (c) and (d) for the COSMIC profile measured on July 12, 2007 at 20:09:19 UT at Lat = 64.84° S and Lon = 96.76° W.

C. Up To What Altitude Can the Linear Approximation of the Topside Scale Height Be Considered Appropriate?

In Section IV-A, we have demonstrated that by considering only the first-order term in the Taylor expansion of the topside scale height as modeled by NeQuick (i.e., considering a linear dependence on the altitude), it is possible to reliably reproduce the topside profile as recorded by COSMIC satellites. However, it is still an open question up to what altitude above $hmF2$ the linear approximation of the topside scale height is reasonable. Obviously, relationship (10) has been derived by expanding the NeQuick topside scale height around $hmF2$, so the accuracy of the Taylor expansion decreases getting away from $hmF2$ and we need to add terms of higher-order to better represent the scale height behavior away from $hmF2$.

Prol *et al.* [39] demonstrated that for a Chapman function, the scale height can also be taken as largely linear in the height range available to COSMIC RO profiles; however, they also demonstrated that there exists a significant departure from this behavior at higher altitudes (above 1000 km), where the scale height exhibits asymptotic behavior, similar to what we would expect from the NeQuick's topside scale height parameterization. It should thus be no surprise that the semi-Epstein layer

of the NeQuick model would similarly exhibit shortcomings at high altitudes when used in the linear regime. It is to the NeQuick's credit that such behavior is modeled by their scale height parameterization, albeit with a suboptimal choice of r and g parameters [29], due to the limited amount of topside electron density profiles available at the time the model was developed.

To provide a first answer to this question, on the left panel of Fig. 8, we have plotted the NeQuick topside scale height obtained through the relationship (2), along with the first four-order terms obtained through the relationship (10). Corresponding electron density values are plotted in the right panel. For each formulation, the following parameters have been considered: $H_0 = 40$ km, $g = 0.2024$, $r = 20$, and $foF2 = 8$ MHz (that is $NmF2 \approx 7.94 \cdot 10^{11}$ el/m³). Specifically, r and g values are those calculated by Themens *et al.* [29]. Fig. 8 points out that the linear approximation can reliably reproduce the NeQuick behavior up to 300 km above $hmF2$. Note that these results depend on the choice of all H_0 , r , and g parameters. For example, considering $g = 0.125$ and $r = 100$, as in the NeQuick model, and again $H_0 = 40$ km, the linear approximation is very good up to about 1000 km above $hmF2$. Indeed higher-order terms are necessary to accommodate the curvature of the topside scale height as modeled by NeQuick. In this case, adding terms up to the fourth

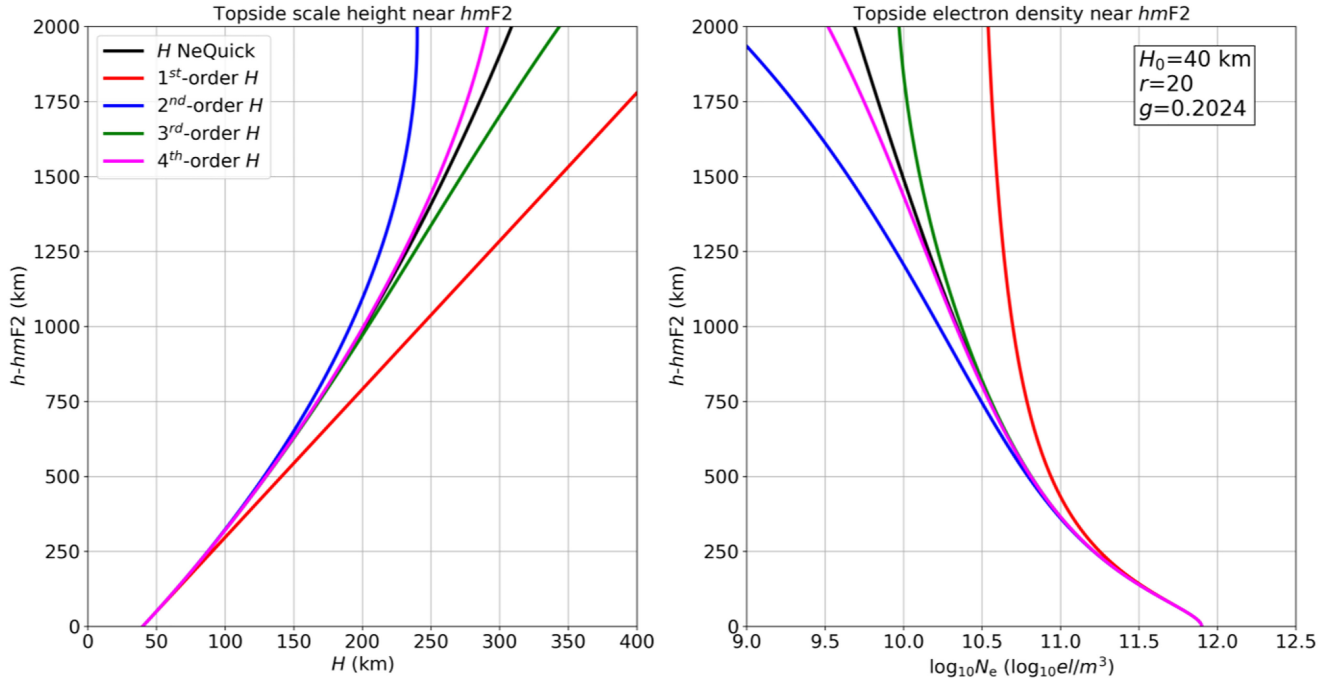


Fig. 8. (Left panel) Topside scale height dependence on altitude near $hmF2$ as modeled by NeQuick through (black line) the relationship (2) and as derived from the Taylor expansion (10) by considering the first-order term (red line), the second-order term (blue line), the third-order term (green line), and the fourth-order term (magenta line). (Right panel) Electron density values calculated by using the topside scale heights of the left panel. The following values have been considered: $H_0 = 40$ km, $g = 0.2024$, $r = 20$, and $foF2 = 8$ MHz, that is $NmF2 \approx 7.94 \cdot 10^{11}$ el/m³.

order, the topside scale height is well reproduced at least up to 1500 km above $hmF2$.

Finally, we can say that for r and g values provided by Themens *et al.* [29] and by setting $H_0 = 40$ km, the linear approximation of the topside scale height can reliably reproduce the topside profile for the altitudes probed by COSMIC satellites, from $hmF2$ to, on average, 300 to 500 km above $hmF2$. Nevertheless, if we want to extrapolate the topside scale height behavior at higher altitudes, the use of the full NeQuick topside scale height formulation (2) is necessary because it implicitly contains the higher order terms also. Here, we only aimed to demonstrate that the linear approximation of the topside scale height cannot be used to represent the entire topside profile but, at the same time, it can be applied if the focus is to obtain a good representation of the lower topside region.

V. CONCLUSION

In this article, the NeQuick topside formulation has been studied in depth to illustrate how the H_0 , r , and g parameters affect the topside scale height formulation and the whole NeQuick topside electron density description. In addition, a fully analytical formulation of the topside scale height, derived by inverting the NeQuick semi-Epstein formulation, has been applied to selected COSMIC RO profiles.

We have highlighted how the H_0 parameter is the most important one because it affects the entire topside profile, from $hmF2$ to infinity. This is the reason why many efforts focused on this parameter when trying to improve the NeQuick topside formulation [14], [26], [29]. It has been demonstrated how the g parameter affects the topside scale height behavior especially in

the lowest topside region. By considering a selected dataset made by 382 COSMIC RO profiles, H_0 and g values have been derived through a linear fit of retrieved topside scale height values, as the corresponding intercepts and slopes; this approach allows us to get very reliable H_0 and g values from COSMIC (or other missions') RO profiles and also from ISR topside profiles.

When considering only the lowest topside region (from $hmF2$ to about 800 km of altitude), this study showed that the linear approximation of the topside scale height, embedded in NeQuick, is very reliable. However, to describe the entire topside profile the use of higher order terms is essential. With regard to this issue, in the NeQuick model, the topside behavior for altitudes well above $hmF2$ is taken into account through the inclusion of the r parameter. However, retrieving information on the r parameter from COSMIC RO profiles is not feasible because higher order terms have a very little importance at COSMIC probed altitudes.

This article, studying in depth some features of the NeQuick topside formulation, complements the existing literature about the model and consequently it is considered beneficial for NeQuick and IRI users interested in the topside modeling.

ACKNOWLEDGMENT

The authors would like to thank the Telecommunications/ICT for Development (T/ICT4D) Laboratory team of the Abdus Salam International Centre for Theoretical Physics (Trieste, Italy), for developing, maintaining, and making available the NeQuick model.¹

¹Online. [Available]: <https://t-ict4d.ictp.it/nequick2/nequick-2-web-model>

Thanks are due to the COSMIC/FORMOSAT-3 team for making freely available Radio Occultation data by means of COSMIC Data Analysis and Archive Center (CDAAC).²

This publication uses data from ionospheric observatories made available via the public access portal of the Digital Ionogram Database³ of the Global Ionosphere Radio Observatory in Lowell, MA. The authors are indebted to the observatory directors and ionosonde operators for the significant investments of their time, effort, expertise, and funds needed to acquire and provide measurement data to academic research.

REFERENCES

- [1] H. Rishbeth and O. Garriott, *Introduction to Ionospheric Physics*. New York, NY, USA: Acad. Press, 1969.
- [2] S. A. Pulinets, V. H. Depuev, A. T. Karpachev, S. M. Radicella, and N. P. Danilkin, "Recent advances in topside profile modeling," *Adv. Space Res.*, vol. 29, no. 6, pp. 815–823, 2002.
- [3] B. W. Reinisch, P. Nsumei, X. Huang, and D. K. Bilitza, "Modeling the F2 topside and plasmasphere for IRI using IMAGE/RPI and ISIS data," *Adv. Space Res.*, vol. 39, no. 5, pp. 731–738, 2007.
- [4] R. F. Benson, D. Bilitza, S. F. Fung, V. Truhlik, and Y. Wang, "Enhancing the ISIS-1 topside digital ionogram database," *Radio Sci.*, vol. 53, no. 12, pp. 1492–1505, 2018.
- [5] J. B. Habarulema, and N. Ssessanga, "Adapting a climatology model to improve estimation of ionosphere parameters and subsequent validation with radio occultation and ionosonde data," *Space Weather*, vol. 15, no. 1, pp. 84–98, 2017.
- [6] L. Liu, W. Wan, M.-L. Zhang, B. Ning, S.-R. Zhang, and J. M. Holt, "Variations of topside ionospheric scale height over Millstone Hill during the 30-day incoherent scatter radar experiment," *Ann. Geophys.*, vol. 25, pp. 2019–2027, 2007.
- [7] L. Liu, H. Le, W. Wan, M. P. Sulzer, J. Lei, and M.-L. Zhang, "An analysis of the scale heights in the lower topside ionosphere based on the Arecibo incoherent scatter radar measurements," *J. Geophys. Res. Space Phys.*, vol. 112, 2007, Art. no. A06307.
- [8] D. R. Themens, P. T. Jayachandran, M. J. Nicolls, and J. W. MacDougall, "A top to bottom evaluation of IRI 2007 within the polar cap," *J. Geophys. Res., Space Phys.*, vol. 119, no. 8, pp. 6689–6703, 2014.
- [9] M. Nigussie, S. M. Radicella, B. Damtie, E. Yizengaw, B. Nava, and L. Roininen, "Validation of NeQuick TEC data ingestion technique against C/NOFS and EISCAT electron density measurements," *Radio Sci.*, vol. 51, pp. 905–917, 2016.
- [10] J. K. Hargreaves, *The Solar-Terrestrial Environment*. Cambridge, U.K.: Cambridge Univ. Press, 1992.
- [11] D. Bilitza et al., "International Reference Ionosphere 2016: From ionospheric climate to real-time weather predictions," *Space Weather*, vol. 15, pp. 418–429, 2017.
- [12] B. Nava, P. Coisson and S. M. Radicella, "A new version of the NeQuick ionosphere electron density model," *J. Atmos. Sol. Terrestrial Phys.*, vol. 70, pp. 1856–1862, 2008.
- [13] D. Bilitza, "Evaluation of the IRI-2007 model options for the topside electron density," *Adv. Space Res.*, vol. 44, pp. 701–706, 2009.
- [14] P. Coisson, S. M. Radicella, R. Leitinger, and B. Nava, "Topside electron density in IRI and NeQuick: Features and limitations," *Adv. Space Res.*, vol. 37, pp. 937–942, 2006.
- [15] A. Pignalberi, M. Pezzopane, R. Tozzi, P. De Michelis, and I. Coco, "Comparison between IRI and preliminary Swarm Langmuir probe measurements during the St. Patrick storm period," *Earth, Planets Space*, vol. 68, p. 93, 2016.
- [16] A. Pignalberi, M. Pezzopane, and R. Rizzi, "Modeling the lower part of the topside ionospheric vertical electron density profile over the European region by means of Swarm satellites data and IRI UP method," *Space Weather*, vol. 16, pp. 304–320, 2018.
- [17] S. Chapman, "The absorption and dissociative or ionizing effect of monochromatic radiation in an atmosphere on a rotating earth," *Proc. Phys. Soc.*, vol. 43, no. 1, pp. 26–45, 1931.
- [18] P. S. Epstein, "Reflection of waves in an inhomogeneous absorbing medium," *Proc. Nat. Acad. Sci. USA*, vol. 16, no. 10, pp. 627–637, 1930.
- [19] K. Rawer, "Replacement of the present sub-peak plasma density profile by a unique expression," *Adv. Space Res.*, vol. 2, no. 10, pp. 183–190, 1982.
- [20] R. Leitinger, S. Radicella, G. Hochegger, and B. Nava, "Diffusive equilibrium models for the height region above the F2 peak," *Adv. Space Res.*, vol. 29, no. 6, pp. 809–814, 2002.
- [21] C. Fonda, P. Coisson, B. Nava, and S. M. Radicella, "Comparison of analytical functions used to describe topside electron density profiles with satellite data," *Ann. Geophys.*, vol. 48, no. 3, pp. 491–495, 2005.
- [22] M. L. Zhang, S. M. Radicella, L. Kersley, and S. A. Pulinets, "Results of the modeling of the topside electron density profile using the Chapman and Epstein functions," *Adv. Space Res.*, vol. 29, no. 6, pp. 871–876, 2002.
- [23] D. Bilitza and B. Reinisch, "International Reference Ionosphere 2007: Improvements and new parameters," *Adv. Space Res.*, vol. 42, no. 4, pp. 599–609, 2008.
- [24] P. Coisson, B. Nava, and S. M. Radicella, "On the use of NeQuick topside option in IRI-2007," *Adv. Space Res.*, vol. 43, no. 11, pp. 1688–1693, 2009.
- [25] R. Leitinger, M. L. Zhang, and S. M. Radicella, "An improved bottomside for the ionospheric electron density model NeQuick," *Ann. Geophys.*, vol. 48, no. 3, pp. 525–534, 2005.
- [26] M. Pezzopane and A. Pignalberi, "The ESA Swarm mission to help ionospheric modeling: A new NeQuick topside formulation for mid-latitude regions," *Sci. Rep.*, vol. 9, 2019, Art. no. 12253.
- [27] E. Friis-Christensen, H. Lühr, and G. Hulot, "Swarm: A constellation to study the Earth's magnetic field," *Earth, Planets Space*, vol. 58, pp. 351–358, 2006.
- [28] D. J. Knudsen *et al.*, "Thermal ion imagers and Langmuir probes in the Swarm electric field instruments," *J. Geophys. Res. Space Phys.*, vol. 122, pp. 2655–2673, 2017.
- [29] D. R. Themens *et al.*, "Topside electron density representations for middle and high latitudes: A topside parameterization for E-CHAIM based on the NeQuick," *J. Geophys. Res., Space Phys.*, vol. 123, pp. 1603–1617, 2018.
- [30] D. R. Themens, P. T. Jayachandran, and R. H. Varney, "Examining the use of the NeQuick bottomside and topside parameterizations at high latitudes," *Adv. Space Res.*, vol. 61, no. 1, pp. 287–294, 2017.
- [31] J. J. Angerami and J. O. Thomas, "Studies of planetary atmospheres: 1. The distribution of electrons and ions in the Earth's exosphere," *J. Geophys. Res.*, vol. 69, no. 21, pp. 4537–4560, 1964.
- [32] R. A. Anthes *et al.*, "The COSMIC/FORMOSAT-3 Mission: Early results," *Bull. Amer. Meteorol. Soc.*, vol. 89, pp. 313–333, 2008.
- [33] J. B. Habarulema, Z. T. Katamzi and E. Yizengaw, "A simultaneous study of ionospheric parameters derived from FORMOSAT-3/COSMIC, GRACE, and CHAMP missions over middle, low, and equatorial latitudes: Comparison with ionosonde data," *J. Geophys. Res. Space Phys.*, vol. 119, pp. 7732–7744, 2014.
- [34] Y. H. Chu, C. L. Su, and H. T. Ko, "A global survey of COSMIC ionospheric peak electron density and its height: A comparison with ground-based ionosonde measurements," *Adv. Space Res.*, vol. 46, pp. 431–439, 2010.
- [35] B. W. Reinisch and I. A. Galkin, "Global Ionospheric Radio Observatory (GIRO)," *Earth, Planets Space*, vol. 63, pp. 377–381, 2011.
- [36] M. M. Shaikh, B. Nava, and H. Haralambous, "On the use of topside RO-derived electron density for model validation," *J. Geophys. Res. Space Phys.*, vol. 123, 2018, Art. no. A025132.
- [37] K. M. Laundal, and A. D. Richmond, "Magnetic coordinate systems," *Space Sci. Rev.*, vol. 206, pp. 27–59, 2017.
- [38] V. Depuev, and S. Pulinets, "A global empirical model of the ionospheric topside electron density," *Adv. Space Res.*, vol. 34, no. 9, 2016–2020, 2004.
- [39] F. Prol, D. R. Themens, M. Hernández-Pajares, P. de Oliveira Camargo, and M. T. de Assis Honorato Muella, "Linear Vary–Chap topside electron density model with topside sounder and radio-occultation data," *Surv. Geophys.*, vol. 40, pp. 277–293, 2019.
- [40] M. Hernández-Pajares *et al.*, "Electron density extrapolation above F2 peak by the linear Vary–Chap model supporting new Global Navigation Satellite Systems-LEO occultation missions," *J. Geophys. Res. Space Phys.*, vol. 122, pp. 9003–9014, 2017.
- [41] M. Garcia-Fernandez, M. Hernandez-Pajares, J. M. Juan, and J. Sanz, "Improvement of ionospheric electron density estimation with GPSMET occultations using Abel inversion and VTEC information," *J. Geophys. Res. Space Phys.*, vol. 108, p. 1338, 2003.
- [42] X. Wu, H. Hu, X. Gong, X. Zhang, and X. Wang, "Analysis of inversion errors of ionospheric radio occultation," *GPS Solutions*, vol. 13, pp. 231–239, 2009.
- [43] X. Yue *et al.*, "Error analysis of Abel retrieved electron density profiles from radio occultation measurements," *Ann. Geophys.*, vol. 28, no. 1, pp. 217–222, 2010.

²Online. [Available]: <http://cdaac-www.cosmic.ucar.edu/cdaac/products.html>

³Online. [Available]: <http://ulcar.uml.edu/DIDBase/>



Alessio Pignalberi received the B.S. and M.S. degrees in physics from the “Sapienza” University of Rome, Rome, Italy, in 2011 and 2014, respectively, and the Ph.D. degree in geophysics from the “Alma Mater Studiorum” University of Bologna, Bologna, Italy, in 2019, by defending a thesis on “A three-dimensional regional assimilative model of the ionospheric electron density.”

He is currently a Postdoctoral Researcher with Istituto Nazionale di Geofisica e Vulcanologia, Rome, Italy. He has authored of 15 articles. His main research interests include the development, implementation, and validation of data-assimilation empirical ionospheric models. Other research interests include the modeling of the ionosphere vertical electron density profile (above all the topside part), the study of the ionospheric Sporadic E layer and of small-scale properties of ionospheric plasma.



Michael Pezzopane received the M.Sc. degree in physics from the “Sapienza” University of Rome, Rome, Italy, in 1997, and the Ph.D. degree in geophysics from the “Alma Mater Studiorum” University of Bologna, Bologna, Italy, in 2005.

Since 2001, he has been a Geophysicist with the Istituto Nazionale di Geofisica e Vulcanologia, Upper Atmosphere Physics and Radiopropagation Unit, Rome, Italy. He has authored or coauthored more than 80 papers published in scientific peer-reviewed journals. His main research interests include ionospheric

physics, radio wave propagation in the ionosphere, atmospheric gravity waves, autoscaling of vertical ionospheric soundings, electron density irregularities at low latitudes, E sporadic layer, topside modeling, and three-dimensional electron density modeling of the ionosphere.

Dr. Pezzopane is a topical Editor for *Annals of Geophysics* and a member of the International Reference Ionosphere Working Group.



David R. Themens received the M.Sc. degree in atmospheric and oceanic science from McGill University, Montreal, QC, Canada, in 2013, and the Ph.D. degree in radio and plasma physics from the University of New Brunswick, Fredericton, NB, in 2018.

He is currently a Postdoctoral Fellow with the University of New Brunswick, where he serves as the Project Lead for the Empirical Canadian High Arctic Ionospheric Model. His research interests include empirical ionospheric modeling, data assimilation, radio propagation, and the study of ionosphere–atmosphere coupling at high latitudes.



Haris Haralambous received the Ph.D. degree in digital communications from the University of Manchester Institute of Science and Technology, Manchester, U.K., in 2003.

He is an Assistant Professor with the Electrical Engineering Department, Frederick University, Nicosia, Cyprus, and the Head of the Ionospheric Research Group, Frederick University, Cyprus. His research interests include ionospheric and space weather effects on radio systems as well as ionospheric morphology studies using ionosondes, global navigation satellite systems, and radio occultation techniques.



Bruno Nava received the M.Sc. degree in physics from the University of Trieste, Trieste, Italy, in 2000.

He is a Research Officer with the Abdus Salam International Centre for Theoretical Physics (ICTP), Trieste, Italy. In collaboration with his colleagues at ICTP and Graz University, Austria, he has developed the ionosphere electron density model NeQuick. He has authored more than 40 papers in peer-reviewed journals and has been involved in several national and international research projects. His research interests include three-dimensional and time-dependent ionospheric

electron density models, data assimilation into ionospheric models, and GNSS Radio Occultation data inversion.



Pierdavid Coisson received the Master’s degree in physics from the University of Trieste, Trieste, Italy, in 2002, and the Ph.D. degree in geophysics from the Institut de physique du globe de Paris, Paris, France, in 2012.

He was with the Abdus Salam International Centre for Theoretical Physics, Trieste, Italy, developing the topside model that was included into NeQuick 2 and IRI 2007. He is currently an Associate Physicist with the French National Magnetic Observatory, Chambon la forêt, France. His research interests include

ionospheric empirical modeling, coseismic ionospheric seismology, ground and space magnetometry, and ionospheric radio propagation from ELF to UHF frequencies.